Research Journal of Applied Sciences, Engineering and Technology 3(6): 558-568, 2011
ISSN: 2040-7467

Received: May 21, 2011 Accepted: June 20, 2011 Published: June 25, 2011

A New Iris Segmentation Method Based on Improved Snake Model and Angular Integral Projection

Ann A. Jarjes, Kuanquan Wang and Ghassan J. Mohammed
School of Computer Science and Technology, Harbin Institute of Technology (HIT), Harbin-150001, China

Abstract: Segmenting iris region is fundamental for iris-based biometric systems. The overall performance of an iris recognition system is highly dependent on accurate iris segmentation. In this paper, a new algorithm for iris segmentation is proposed towards more accurate and efficient segmentation, it detects the precise pupil contour and localizes the limbic boundary. An improved snake model is presented, wherein a new external energy function is designed. This external energy is computed based on the Angular Integral Projection Function (AIPF). First, the AIPF is combined with the improved snake to detect the pupil boundary. For that, pupil boundary points are detected by using the AIPF, and circle fitting is followed to localize the circular pupil boundary giving the initial snake contour. Then, the precise pupil contour is detected by deploying the improved snake. Second, as another contribution of this work, the limbic boundary is localized by combining the AIPF with a technique to extract outlier boundary points based on Mahalanobis distance. Experimental results on CASIA V3.0 iris image database show that the improved snake model is comparable with conventional snake model, and the whole segmentation performance of the proposed algorithm outperforms those of other well-known existing methods in both terms of accuracy and processing time.

Key words: Active contour model, angular integral projection, biometrics, Iris segmentation, boundary detection, external energy field

INTRODUCTION

In recent years, automatic personal identification is more concerned with biometrics recognition technology. Biometric technology is an automated method for identifying individuals based on their behavioral (signature, gait, voice, etc.) or physical (face, iris, finger print, palm print, etc.) characteristics. The iris is the colored portion of the eye that is located between the white sclera and black pupil, it is considered to be the most reliable and accurate biometric due to the richness, uniqueness, and stability of its texture. Hence, iris recognition which identifies people based on Iris, is now one of the most accurate and effective biometric identification systems (Daugman, 1993). The first and probably the most important step in an iris recognition system is iris segmentation, which aims to detect the iris inner boundary (between pupil and iris) and iris outer boundary (between iris and sclera). Other subsequent feature extraction and matching steps are closely related to the precision of the iris segmentation; consequently, the overall performance of iris recognition system is highly dependent on the segmentation accuracy. The two well-known methods of iris localization are attributed to Daugman (1993) and Wildes (1997). Where, Daugman proposed an integrodifferential operator to localize both iris inner and outer boundaries, and Wildes localized the iris through edge points detection with voting procedure realized via Hough transform. Since the above two prominent works, many others modified methods for iris segmentation have been developed. Ma *et al*. (2003) presented an iris segmentation method by using edge detection together with Hough transform. Huang *et al*. (2004) extracted edge information based on phase congruency then segmented iris using Hough transform. Masek (2003) also segmented iris by combining Canny edge detection with Hough transform. Tisse *et al*. (2002) proposed a segmentation method based on integrodifferential operator with Hough transform, and Cui *et al*. (2004) used Haar wavelet transform followed by Hough transform for detecting iris inner boundary and differential integral operator for localizing iris outer boundary. With more interest in iris recognition, other improved algorithms have been recently proposed in (He and Shi, 2007; Sudha *et al*., 2009; Chen *et al*., 2010). An excellent review of these methods is recently presented by Bowyer *et al*. (2008). Despite of the varieties in the above mentioned methods, they have several drawbacks. Firstly, most of these algorithms are based on edge detection together with Hough transform, which makes the process

Corresponding Author: Ann A. Jarjes, School of Computer Science and Technology, Harbin Institute of Technology (HIT), Harbin-150001, China

time-consuming. Secondly, almost all these algorithms assume pupil boundary as a circular contour and fit a circle to it, which is not true in all cases. Errors in localizing pupil boundary through fitting a circle can result in inferior performance for iris matching, since most discriminative iris information exists in the collarette which is small area around the pupil. And lastly, the drawback of the possible failure to detect the pupil and iris circles, since most mentioned localization algorithms require threshold values to be set for edge detection and this may cause critical edge points being removed. In the recent ten years, active contour model, also called snake, has been extensively studied and successfully applied in many fields, including computer vision, object detection, and object motion. The basic idea of the active contour that is based on energy minimization function, first introduced by Kass *et al*. (1987), is to evolve a snake curve from an initial state under the combined influence of internal force, image force, and external constraint force. However, traditional active contour models have few disadvantages, including the sensitiveness to the initial contour and the speed of convergence. Another central problem is the choice of the snake external force, since different types of external force lead to different image features. Addressing these limitations, another improved implementation of the snake model based on greedy optimization algorithm was proposed by Williams and Shah (1992), it significantly increased the speed of convergence, but it was more sensitive to the initial contour location.

In this study, a new algorithm for iris segmentation is presented. Based on the original snake model (Kass *et al*., 1987), an improved snake model is proposed to accurately detect the pupil contour. Here, to provide more proper and realistic representation of external energy that is well-related to the object under consideration (pupil contour), a new external energy model is designed based on the Angular Integral Projection Function (AIPF). In our previous study (Mohammed *et al*., 2010), the AIPF has been proposed as a general function to perform integral projection along angular directions. The proposed algorithm of iris segmentation is composed mainly of two stages. In the first stage, the accurate pupil boundary is detected. Firstly, the pupil center is approximated as the center of mass of the binarized iris image, then, a set of pupil boundary points is detected by applying the AIPF basing on the approximated pupil center. Secondly, an initial contour for the improved snake is localized by fitting a circle to the above detected boundary points. Finally, the improved snake model is deployed to detect the accurate pupil contour. Here, it should be pointed out that, the high performance of the detection of the pupil parameters using the AIPF, reported in (Mohammed *et al*., 2010), implies that the proposed initial contour is well-localized near the true pupil contour. Hence, the proposed algorithm has solved the conventional problem of the snake sensitiveness to the initial contour. Experiments indicate that the improved snake model has obtained slight performance improvement in terms of accuracy and computation time when applied based on both the classical snake algorithm (Kass *et al*., 1987), and greedy snake algorithm (Williams and Shah, 1992). While, in the second stage of the proposed algorithm, the limbic boundary is localized. Here, considering the pupil center detected in the previous stage as the approximated iris center, and after iris image being filtered, the AIPF is applied again to detect a set of iris boundary points in both iris' left and right sides. Then, based on the measured Mahalanobis distances of these points form the approximated iris center, noisy boundary points are identified and excluded. Lastly, the limbic boundary is localized through fitting a circle to the remaining boundary points. As the objective of this paper is to improve iris segmentation based on new proposed algorithm, experimental results provide that the proposed algorithm is more efficient and accurate as compared with some best known existing methods for iris segmentation, such as Daugman's integrodifferential operator (Daugman, 1993) and Masek algorithm (Masek, 2003), where all experiments for iris segmentation are performed on iris images from CASIA V3.0 database (CASIA, 2006).

ORIGINAL SNAKE MODEL

An active contour model or snake, since it was first proposed by Kass *et al*. (1987), has been widely applied to detect and segment the contour of an object of interest. A snake is defined as energy minimization method, it iteratively evolves by minimizing an energy functional $E_{snake}(\mathbf{v}(s))$. In each iteration, the new snake curve is that with the lower energy and better matches to the target object contour than the initial contour. Representing the position of a snake parametrically as:

$$\mathbf{v}(s) = [x(s), y(s)] \text{ for } s \in [0, 1]$$

the energy functional is defined as follows:

$$E_{snake}(v(s)) = \int_{s=0}^{1} E_{\text{int}}(v(s)) + E_{img}(v(s)) + E_{con}(v(s))ds \quad (1)$$

The first energy term $E_{int}(\mathbf{v}(s))$ represents the internal energy and is given by:

$$E_{\text{int}}(v(s)) = \frac{1}{2}\left(\alpha(s)\|v_s(s)\|^2 + \beta(s)\|v_{ss}(s)\|^2\right) \quad (2)$$

where the first-order term $\|v_s(s)\|^2$ provides a measure of snake continuity and the second-order term $\|v_{ss}(s)\|^2$ provides a measure of snake curvature. The influence of these two terms is controlled by the parameters α(*s*) and β(*s*). The external energy function is composed of the second and third energy terms in Eq. (1). Where the second energy term E_{image} (**v**(*s*)) represents the image energy which attracts the snake to the desired low-level features in the image, it is conventionally defined as:

$$E_{img}(v(s)) = -\left\|\nabla\left[G_\sigma(x,y) * I(x,y)\right]\right\|^2 \quad (3)$$

where $I(x,y)$ is the image function and $G_\sigma(x,y)$ is a two dimensional Gaussian with standard deviation σ, which is convolved with I for the purpose of noise removing and increasing the snake capture range. While the other term E_{con} (**v**(*s*)) refers to the external constraints and it is optional. Solving the optimization with Euler-Lagrange equation, will result in the following differential equation:

$$\alpha(s)v_{ss}(s) + \beta(s)v_{ssss}(s) + \frac{\partial E_{image}}{\partial s} = 0 \quad (4)$$

After substituting the derivatives in Eq. (4) with the finite difference approximations, and then solving the equation iteratively in matrix form, the final solution for the snake evolution is given as:

$$v_{t+1} = (A + \gamma I)^{-1}(\gamma v_t + f(v_t)) \quad (5)$$

where the coefficient matrix A contains the derivative terms, I is the identity matrix, $f(\mathbf{v}_t)$ is the image energy of the snake curve $\mathbf{v}_t$ in the *t*th iteration, and g is the step size.

IMPROVED SNAKE MODEL

Regarding the limitations of the traditional snake model, and considering the characteristics of the object of interest, an improved snake model based on the original snake is introduced. New external energy field is designed to effectively attract the snake curve and locate it over the object contour. The new external field is derived from image data by using AIPF. Where, the AIPF has been recently proposed in (Mohammed *et al*., 2010), and proved its efficiency to detect pupil features. The definition of the AIPF and the implementation of the proposed external energy field are presented in the following sub-sections.

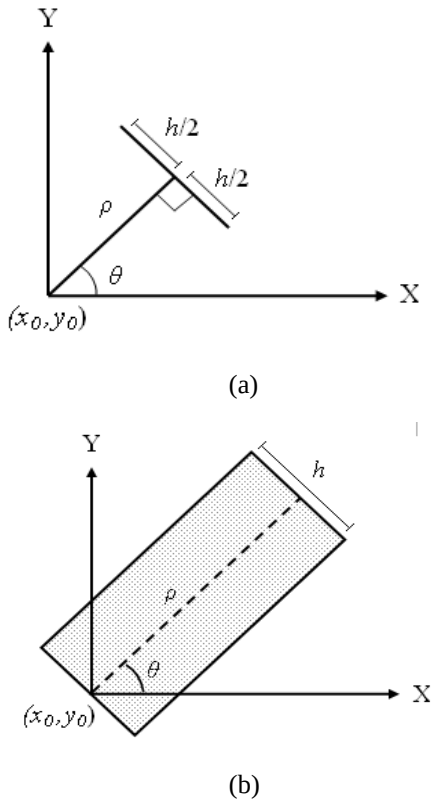

Fig. 1: Definition of AIPF parameters, (a) Line parameters; (b) Integration rectangle

Angular integral projection function: As a general function to perform localized integral projection along angular directions within image space, the Angular Integral Projection Function (AIPF) has been proposed in our earlier work (Mohammed *et al*., 2010) and applied, in particular, to detect boundary points between different image regions. Within image space, the AIPF computes the integral of each line described by the parameters: θ is the angle of the line normal with *x*-axis, ρ is the distance from the image center to the line, and *h* represents the number of points within the line. Given these parameters, as shown in Fig. 1, the AIPF is defined as follows:

$$AIPF(\theta,\rho,h) = \frac{1}{h+1}\int_{j=-h/2}^{h/2} I\Big(\big(x_0 + \rho\cos\theta\big) + \Big(j\cos\big(\theta + \tfrac{\pi}{2}\big)\Big), \big(y_0 + \rho\sin\theta\big) + \Big(j\sin\big(\theta + \tfrac{\pi}{2}\big)\Big)\Big)dj \quad (6)$$

where (x_0, y_0) is the image center and $I(x, y)$ represents the gray level of the pixel at location (x, y). Then, it is easy to

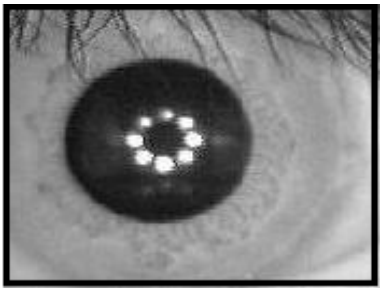

(a)

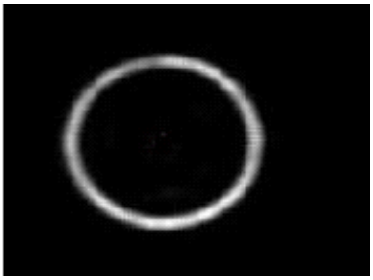

(b)

Fig. 2: Evaluating the new external energy model, (a) Pupil image; (b) External energy field

notice, that the application of AIPF for ρ = 0, 1, …, *w*, will yield an integration rectangle with *h*×*w* dimensions and having θ with *x*-axis. Also it should be pointed out, that even the most commonly used vertical integral projection function IPF_v and horizontal integral projection function IPF_h can be implemented using the AIPF by assigning $\theta = 0°,180°$ and $\theta = 90°, 270°$, respectively.

New external energy model based on AIPF: The proposed external energy model is implemented by setting a new definition for the image energy function in Eq. (3). Where, the new image energy term is implemented by mapping the image domain into a new transformed domain based on the AIPF. Mapping to the new domain is performed, such that each point in the new domain represents the gradient of the sum of pixels intensity within a column has: *h* height, ρ offset from the image center, and its normal has θ with *x*-axis. Then, in order to reduce the effect of potential noise and increase the capture range of the snake, the new domain is convolved with Gaussian kernel. Given a gray level image $I(x, y)$, the proposed new energy function could be written as:

$$E_{img} = -\left(\nabla\left[AIPF_{\theta,\rho,h,x_0,y_0}\left(I(x,y)\right)\right]^2 * G_\sigma(x,y)\right) \quad (7)$$

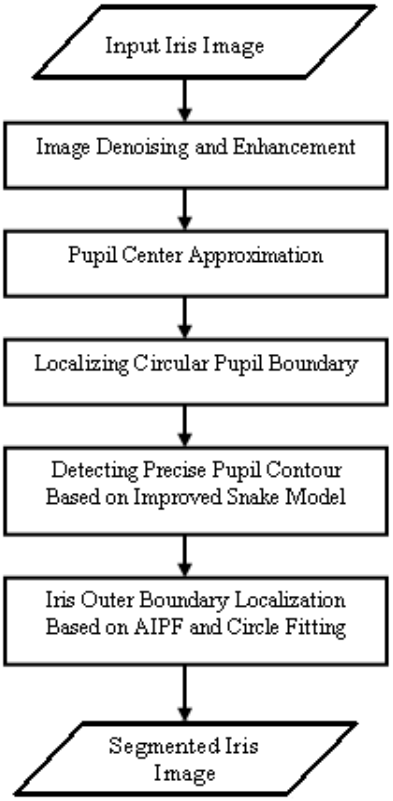

Fig. 3: The flow diagram of the proposed algorithm

where $AIPF_{(\theta,\rho,h,x0,y0}$ computes the angular integral projection along all lines characterized by the parameters (θ, ρ, *h*) within image space have (x_0, y_0) center. $G_\sigma(x, y)$ is a two dimensional Gaussian function with standard deviations, σ, ∇ is the gradient operator, and * represents the convolution. Figure 2 shows the new image energy field computed based on Eq. (7).

PROPOSED IRIS SEGMENTATION ALGORITHM

The proposed algorithm for iris segmentation is presented in this section. It consists of five steps as shown in Fig. 3, and briefly described in the following. In the first step, image denoising and enhancement, image specular spots are removed, then, the iris image is filtered. In the second step, the pupil center is approximated. While in the third step, the circular pupil boundary is localized. Then in the fourth step, being initialized on the localized circular boundary, the improved snake model is applied to detect the precise pupil contour. And finally, the outer iris boundary is localized in the fifth step.

Image denoising and enhancement: Commonly, iris images obtained from CASIA V3.0 are contaminated with several specular spots within pupil region; these spots

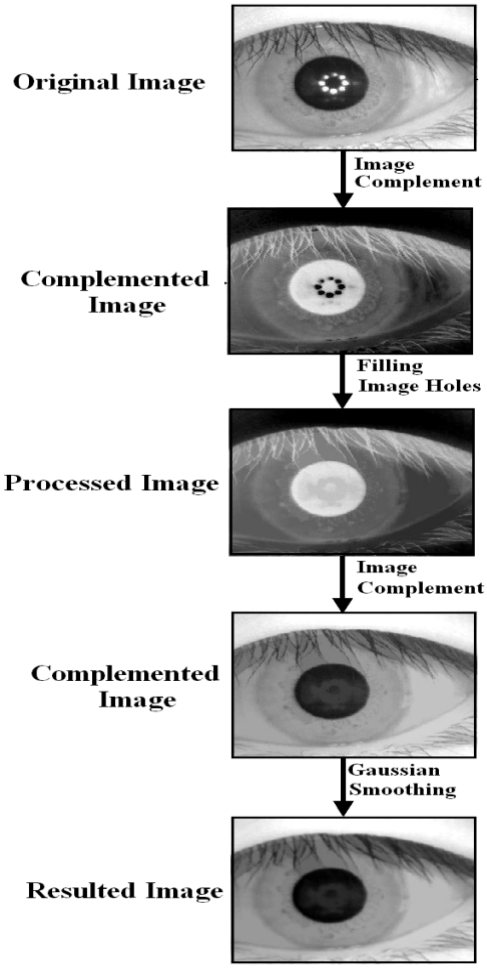

Fig. 4: Image denoising and enhancement

were caused by the NIR illuminators used to capture iris images. These noisy spots can result in failure to detect pupil center and boundary. Therefore, as an initial step, a simple technique with three sub-steps is applied to remove these noisy spots as illustrated in Fig. 4 and explained as follows:

- Finding the complement of the iris image (by calculating the absolute subtraction of each pixel's gray level from 255)
- Filling the resulted dark holes based on connectivity described by 4-connected pixels
- Finally, the complement of the resulted image is evaluated again. However, since the above technique results in sharp image, Gaussian smoothing is followed.

Approximating pupil center: In this step, the pupil region of the preprocessed iris image is segmented in

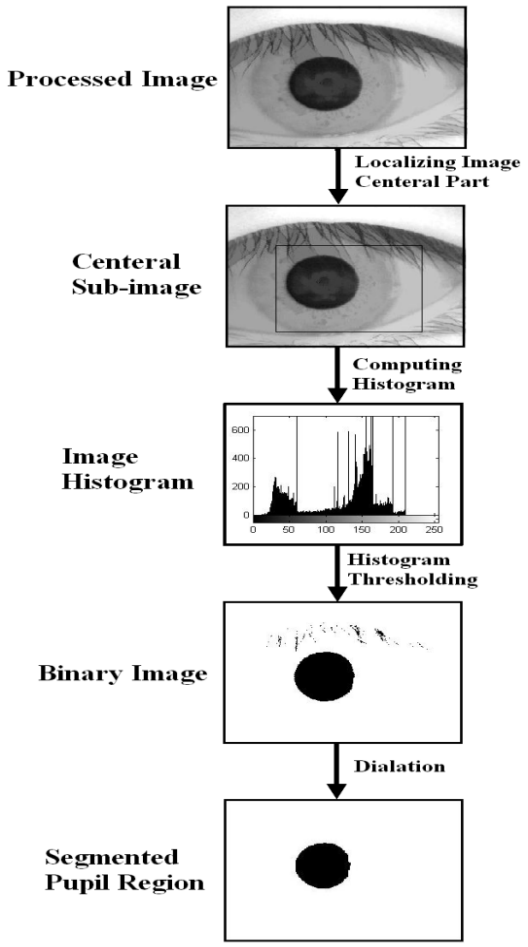

Fig. 5: Approximate pupil center detection

order to detect the approximate pupil center, as illustrated in Fig. 5. First, the gray levels histogram is computed and then analyzed to identify a threshold value T to be applied to create the pupil binary image. Here, to improve the accuracy and processing speed, only the central sub-image which has roughly the half size of the iris image is considered. Then, the pupil binary image is created by setting intensity values in the iris image less or equal T to 0 (black) and otherwise to 255 (white). However, as the resultant binary image still contaminated with noise caused by eyelashes, a morphological operator is applied. Finally, the approximate pupil center (x_p, y_p) is determined as the center of mass of the segmented pupil region, which is obtained as follows:

$$x_p = \frac{1}{\sum g(x,y) \in P} \sum_{g(x,y)\in P} x \quad (8)$$

$$y_p = \frac{1}{\sum g(x,y) \in P} \sum_{g(x,y)\in P} y \quad (9)$$

where $g(x, y)$ is a pixel in the position (x, y), and P represents the segmented pupil.

Pupil segmentation based on AIPF- detecting circular boundary: The circular pupil boundary which acts as the initial contour for the snake to be applied in the next step is localized by applying the AIPF followed by circle fitting. Based on the approximated pupil center, the AIPF is applied to detect a set of pupil boundary points along the whole circumference of the pupil edge that is the parameter θ runs in $[0, 2\pi]$. In detail, a boundary point is obtained for each integration rectangle, which is determined by first computing the gradient of the projection curve that corresponds to the integration rectangle, and then searching the gradient curve for the local maximum that is locating on the pupil edge. Having detected these boundary points, the circular pupil boundary is localized by fitting a circle to these points. For this purpose, the least square method is applied which minimizes the summed square of errors.

Pupil segmentation based on the improved snake-detecting precise pupil contour: Compared to the previous section, the detection of the precise pupil contour is addressed here. The improved snake model with the new external energy field is applied to capture the contour of the pupil region.

Initial contour identifiaction: In (Mohammed *et al*., 2010) as mentioned earlier, it has been proved that the method applied in the previous section to localize the circular boundary, provides high performance. Taking advantage of that and in order to solve the conventional problem, that is, the snake initial contour sholud be selected close to the true bounadry, the initial contour is set on the previously localized pupil circle. This, consequently, will reduce the number of snake iterations and improve the accuracy of the final contour. And for more performance improvement, the number n of the snake control points (snakles) contained in the initial contour is selected proportionally to the pupil circles' radius.

Snake evolution: Prior the snake starts deformation, the challenging task of the determination of the snake parameters arises. Aiming at this problem, extensive experiments have been done, and snake parameters are selected out of wide range of values based on the best results obtained by the snake. These parameters usually include the weighting factors of the snake terms, evolution stopping threshold, maximum number of the snake iterations, and evolution step size. Then, once the initial contour is located, the snake curve is evolved iteratively by minimizing Eq. (1), such that a new snake

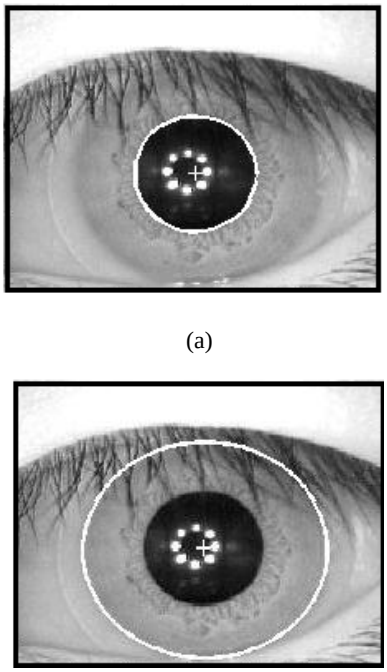

(a)

(b)

Fig. 6: Iris segmentation, (a) Pupil contour detection; (b) Limbic boundary localization

curve with lower energy and better match to the object contour is obtained in each iteration. The snake still deforms until a predefined number m of iterations, or when the average differences between the indices of the snakles at iteration t and iteration t-1 goes under a preselected threshold as in (Tiilikainen, 2007). A detected final contour is shown in Fig. 6a.

Limbus boundary localization: To detect the iris outer boundary, the AIPF is applied here with combination of computing Mahalanobis distances (Duda *et al*., 2001) to detect a set of limbic boundary points. By approximating the iris center as the center of the circle extracted from the final pupil contour detected in the previous section, the proposed algorithm of limbus boundary localization has five steps and is described as follows:

- Within iris image, two iris rectangles are considered to be processed. They established on both iris' left and right sides based on the location of the approximated iris center and the number of integration rectangles to be applied in the iris rectangles. Certainly, this will serve to reduce computational cost and avoid iris regions which are possibly occluded by eyelids and eyelashes.
- And, to minimize the effect of noise particularly caused by eyelashes, a nonlinear filter based on anisotropic diffusion process (Perona and Malik, 1990) is applied within each iris rectangle.

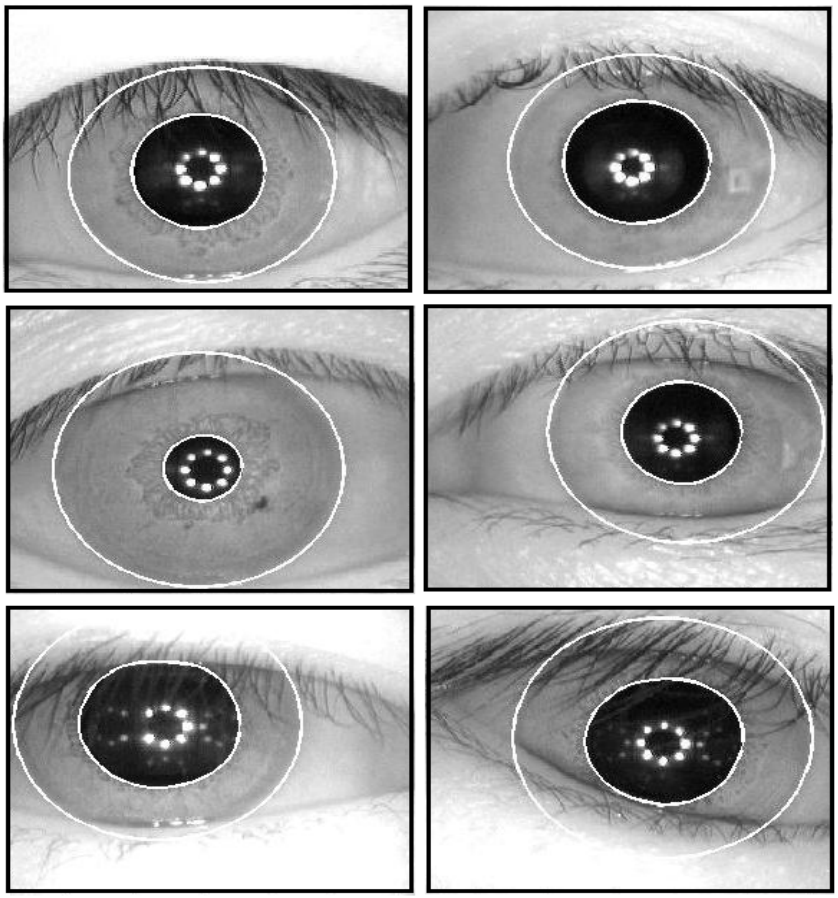

Fig. 7: Segmented iris image samples

- Then, the AIPF is applied for θ runs within the ranges 175°~210° and -30°~5° for the left and right iris rectangles respectively. This is because, within these ranges of θ, the iris image is rarely occluded by eyelashes. Next, similar a set of iris boundary points is detected in each iris rectangle.
- After boundary points are detected, the Mahalanobis distance from each boundary point to the approximated iris center is computed. Based on the computed distance, a threshold value is estimated and, then, applied to identify and exclude outlier's boundary points.
- Finally, the iris outer boundary is localized by fitting a circle to the remaining boundary points by making use of the least square method (Fig. 6b).

EXPERIMENTAL RESULTS AND EVALUATION

In order to investigate the accuracy and efficiency of the proposed algorithm of iris segmentation, extensive experiments are performed on the public iris image database CASIA V3.0 (CASIA, 2006). All the experiments are implemented in MATLAB 7.01 and run on a PC computer with 3 GHz CPU and 1024 MB of memory. The detection accuracy of the both iris boundaries are evaluated based on ground truth method and to perform comparative analysis, two iris localization algorithms are also implemented, one is the prevailing method of the Daugman's integrodifferential operator (1993) and the other is Masek algorithm (Masek, 2003).

Iris image database characteristics: Among several iris image databases available on public, CASIA V3.0 iris database is selected because it provides reliable environment to validate the proposed algorithm since it has 2655 iris images from 249 subjects with 396 total number of iris classes. CASIA V3.0 is collected by the Institute of Automation of the Chinese Academy of Sciences, where most of images were taken in two sessions with at least one month interval. All iris images are 8 bit (256 gray levels) JPEG files with 320×280 pixels size, and collected under infrared illumination.

Performance evaluation method: In contrast to subjective evaluation based on visual inspection which is

Table 1: Performance of pupil contour detection

	Accuracy confidence (%)				
	1- pixel		2- pixel		
Method	center	radius	center	radius	Mean time (s)
Daugman (1993)	80.78	81.12	99.2	98.94	0.78
Masek (2003)	35.11	79.6	83.89	98.37	50.39
Kass snake (Jarjes *et al*., 2010)	90.05	94.57	99.05	99.43	0.40
Improved Greedy snake (Jarjes *et al*., 2011)	85.49	94.3	99.2	99.92	0.35
Proposed snake (Kass)	91.03	95.4	99.13	99.85	0.37

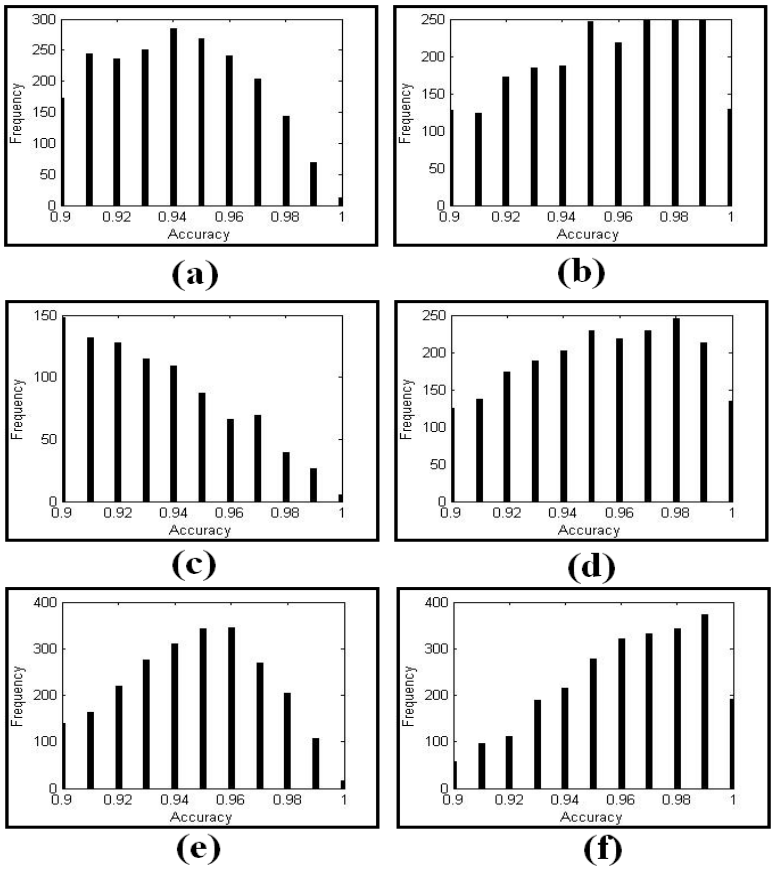

Fig. 8: Accuracy performance of the pupil contour features, (a) Center, (b) Radius for Daugman method, (c) Center, (d) Radius for Masek algorithm, (e) Center, (f) Radius for the proposed algorithm

commonly known as inaccurate, using ground truth approach to evaluate the accuracy of the segmentation results usually provides more reliable measure. Thus, to evaluate the accuracy of the localized two iris boundaries, accurate ground truth is required for each iris boundary. According to the above, ground truth is created separately for each iris boundary, it is composed of the center and radius of the manually localized iris boundary for all iris images within the database. Each ground truth is generated by fitting a circle on the true iris boundary through three steps, as follows:

- As a reference point, an initial center for the true iris boundary is detected and showed, and then an approximate center of the corresponding circle is selected.
- By finding a point located on the true iris boundary, the radius of the corresponding circle is estimated.
- Finally, best circle fitting on the true iris boundary is obtained by precise resizing and positioning the circle defined in the previous two steps.

All above steps, except for the detection of the initial contour, are manually performed. Then, a circularity confidence interval centered at the ground truth pixel with five pixel radius, is defined. Let H (i, j) denote ground truth pixel and E (i, j) the detected pixel. The distance Dis

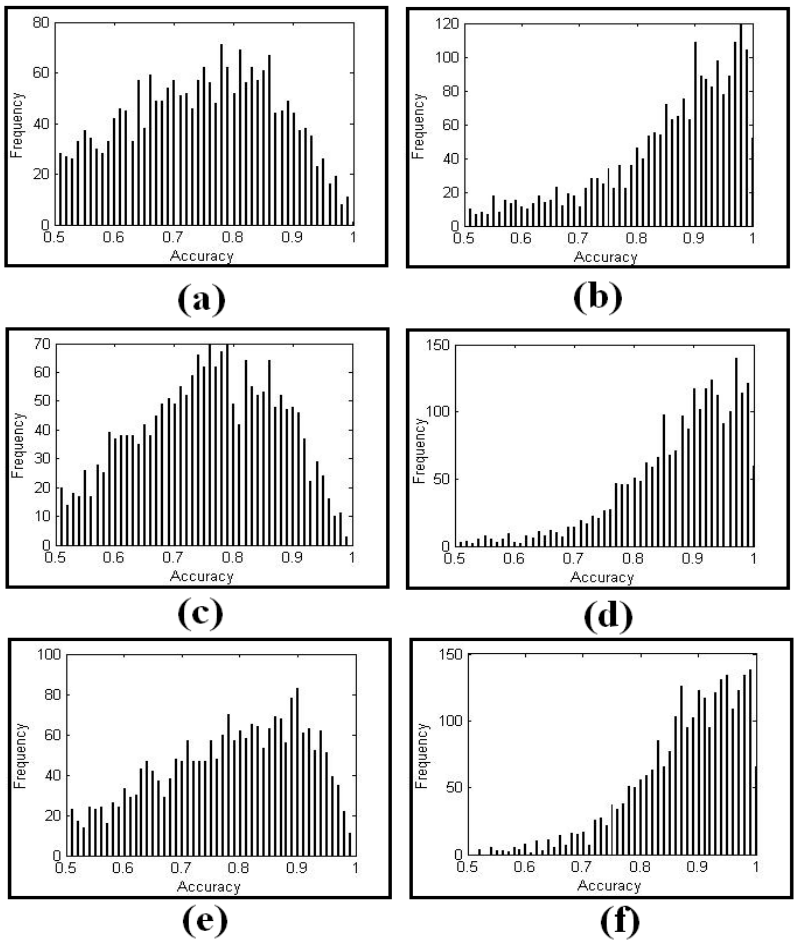

Fig. 9: Accuracy performance of the limbic boundary features, (a) Center, (b) Radius for Daugman method, (c) Center, (d) Radius for Masek algorithm, (e) Center, (f) Radius for the proposed algorithm

of H and E is defined as $\|\text{H-E}\|_2$. And the accuracy of the algorithm is defined as in (Zheng *et al*., 2005):

$$A = \begin{cases} (1 - Dis/5 \times 0.5) \times 100\%, & Dis \le 5 \\ 0, & Dis > 5 \end{cases} \quad (10)$$

where A is set within 50~100% if *Dis* equals or less than the limit of the confidence interval. Otherwise, A is set to 0.

Experiments, analysis and evaluation: This section describes the process of parameters selection. As well as, it gives analysis and evaluation of the accuracy of the localized iris boundaries based on the created ground truth and, also, by comparing with other famous methods in the same field. Two sets of parameters have to be set prior the application of the proposed algorithm, the first is for the AIPF parameters which are selected similar to our previous works in (Mohammed *et al*., 2009, 2010) wherein good localization results have been obtained. While, in the second one, which is the set of the snake's parameters, the parameters are selected empirically out of wide ranges of values depending on the best results obtained for contour detection.

Pupil contour detection: In experiments, and in the process of the detection of the precise pupil contour, the parameters setting: h = 15 pixels, $\Delta\theta$ = 15°, and w = 75 pixels is considered for the application of the AIPF based on our previous work (Mohammed *et al*., 2010). While the parameters setting: α = 0.0006, β = 0.03, Thr(ε) = 0.015, is adopted for the modified snake algorithm, where these parameters have been thoroughly adjusted during extensive experiments. Figure 7 shows the detected final contour for six iris image samples. In order to provide comparative analysis, the performance of the proposed algorithm is firstly compared with those of our earlier works of a new run of the original snake model in

Table 2: Performance of limbic boundary localization

	Accuracy within 5-pixel confidence (%)		
Method	Center	Radius	Mean time (sec)
Daugman (1993)	81.16	80.7	0.95
Masek (2003)	76.25	88.03	18.77
Proposed algorithm	84.8	96.88	0.49

(Jarjes *et al*., 2010), and the improved greedy snake model in (Jarjes *et al*., 2011), since both these models were given the same initial contour as in the proposed algorithm. Second, it is compared with two well-known methods for iris segmentation, Daugman's integrodifferential operator and Masek algorithm. Detailed comparison results are given in Table 1, wherein the accuracy of the localized pupil circle, a circle has been approximated from the snake final contour, has been evaluated within 1-pixel and 2-pixel confidences of ground truth data for both circle features (center, radius). Also, the accuracy performance is explained in Fig. 8.

The localization results are also reported in Table 1. As can be seen from the above experimental results, the proposed algorithm outperforms both methods of Daugman and that of edge detection with Hough transform in terms of accuracy and computational cost; it also provides slight performance improvement over traditional snake model.

Limbic boundary localization: At the stage of limbic boundary localization, the AIPF parameters are selected as h = 15 pixels and w = 75 pixels, and similar to (Mohammed *et al*., 2009), six integration rectangles are generated within each iris rectangle with $\Delta\theta = 5°$. In particular, iris boundary points are detected for ($\theta_1 = 175°$, $\theta_2 = 180°$, $\theta_3 = 185°$, $\theta_4 = 190°$, $\theta_5 = 195°$, $\theta_6 = -200°$) within the left iris rectangle, and for ($\theta_1 = 5°$, $\theta_2 = 0°$, $\theta_3 = -5°$, $\theta_4 = -10°$, $\theta_5 = -15°$, $\theta_6 = -20°$) within the right iris rectangle. Other experimental tests are performed to select a threshold value based on the computed Mahalanobis distances of the detected iris boundary points, then based on the selected threshold, outliers boundary points are detected and excluded. The localization results of various iris images are given in Fig. 7. Similar to the previous section, the methods of Daugman's integrodifferential operator and that of edge detection combined with Hough transform are implemented for the purpose of comparison and, for more reliable comparison, the same approximation of the initial iris center is given for the both proposed method and Daugman's operator. Here, in contrast to the previous section, the accuracy of the localized iris outer boundary is evaluated within 5-pixel confidence of ground truth data. From the results of comparison summarized in Table 2 and the accuracy performance given in Fig. 9, it can be concluded that the proposed method for limbic boundary localization has better performance.

CONCLUSION

Accurate iris segmentation is crucial for iris recognition. New iris segmentation is proposed in this paper for the purpose of performance improvement. An improved snake model is proposed to accurately detect pupil contour, where a new external energy field is designed based on the AIPF which is a general function, as proposed in our earlier work (Mohammed *et al*., 2010), to perform angular integral projection. In addition, a new approach based on the AIPF and Mahalanobis distance is developed to localize iris outer boundary. Extensive experiments performed on CASIA V3.0 and then results evaluation based on ground truth approach, have shown that the proposed algorithm achieves slight performance improvement over traditional snake model. Also, it solves the problem of the snake's sensitiveness to the location of the initial contour. Moreover, as compared with other well-known iris segmentation methods, the proposed algorithm obtains better performance. In the future work, the application of the improved snake model to detect the accurate limbic boundary and eyelids will be investigated. Also, other snake algorithms will be examined based on the proposed external energy field.

ACKNOWLEDGMENT

This study was supported in part by the Natural Science Foundation of China (NSFC) under Contract No. 60872099 and the National High-Tech Research and Development Plan of China (863) under Contract No. 2006AA01Z308.

REFERENCES

Bowyer, K.W., K. Hollingsworth and P.J. Flynn, 2008. Image Understanding for iris biometrics: A survey. Comput. Vis. Image Und., 110: 281-307.

Chen, Y., M. Adjouadi, C. Han, J. Wang, A. Barreto, N. Rishe and J. Andrian, 2010. A highly accurate and computationally efficient approach for unconstrained Iris segmentation. Image Vis. Comput., 28: 261-269.

Chinese Academy of Sciences - Institute of Automation (CASIA), 2006. Iris Image Database (ver. 3.0). Retrieved from: http://www.sinobiometrics.com.

Cui, J., Y. Wang, L. Ma, T. Tan and Z. Sun, 2004. An Iris recognition algorithm using local extreme points. Proc. of International Conference on Biometric Authentication, pp: 442-449.

Daugman, J.G., 1993. High confidence visual recognition of persons by a test of statistical independence. IEEE Trans. Pattern Anal. Mach. Intel., 15: 1148-1161.

Duda, R.O., P.E. Hart and D.G. Stork, 2001. Pattern Classification. 2nd Edn., Wiley-Interscience Publication, Chichester, England.

He, X. and P. Shi, 2007. A new segmentation approach for iris recognition based on hand-held capture device. Pattern Recog., 40: 1326-1333.

Huang, J., Y. Wang, T. Tan and J. Cui, 2004. A New Iris Segmentation Method for Iris. Recognition System. Proceeding of the 17th International Conferance on Pattern Recognition, pp: 554-557.

Jarjes, A.A., K. Wang and G.J. Mohammed, 2010. Iris Localization: Detection Accurate Pupil Contour and Localizing Limbus Boundary. Proceeding of the 2nd CAR 2010, March 6-7, pp: 349-352.

Jarjes, A.A., K. Wang and G.J. Mohammed, 2011. Improved Greedy Snake Model for Detecting Accurate Pupil Contour. Proceeding of the 3rd ICACC 2011, Jan. 18-20, pp: 515-519.

Kass, M., A. Witkin and D. Terzopoulos, 1987. Snakes: Active contour models. Int. J. Comput. Vis., 1: 321-331.

Ma. L., T. Tan, Y. Wang and D. Zhang, 2003. Personal identification based on Iris texture analysis. IEEE Trans. Pattern Anal., 25: 1519-1533.

Masek, L., 2003. Recognition of Human Iris Patterns for Biometric Identification. Retrieved from: http://www.csse.uwa.edu.au/pk/studentprojects/libor.

Mohammed, G.J., B. Hong and A.A. Jarjes, 2009. Eyeball localization based on angular integral projection function. Informatica, 33(4): 475-480.

Mohammed, G.J., B. Hong and A.A. Jarjes, 2010. Accurate pupil features extraction based on new projection function. Comput. Inform., 29(4): 663-680.

Perona, P. and J. Malik, 1990. Scale-space and edge detection using anisotropic diffusion. IEEE Trans. Pattern. Anal., 12: 629-639.

Sudha, N., N.B. Puhan, H. Xia and X. Jiang, 2009. Iris recognition on edge maps. IET Comput. Vis., 3: 1-7.

Tiilikainen, N.P., 2007. A Comparative Study of Active Contour Snakes, Copenhagen University, Denmark

Tisse, C., L. Martin, L. Torres, and M. Robert, 2002. Person Identification Technique Using Human Iris Recognition. Proceeding Vision Interface, pp: 294-299.

Wildes, R.P., 1997. Iris recognition: An emerging biometric technology. Proc. IEEE, 85(4): 1348-1363.

Williams, D.J. and M. Shah, 1992. A fast algorithm for active contours and curvature estimation. Comput. Vis. Graph. Image Process., 55: 14-26.

Zheng, Z., J. Yang and L. Yang, 2005. A robust method for eye features extraction on color image. Pattern Recog. Lett., 26: 2252-2261.